HYDROLOGICAL PROCESSES
Hydrol. Process. **25**, 650–660 (2011)
Published online 7 September 2010 in Wiley Online Library
(wileyonlinelibrary.com) DOI: 10.1002/hyp.7857

Improvement of distributed snowmelt energy balance modeling with MODIS-based NDSI-derived fractional snow-covered area data

Joel W. Homan,[1]* Charles H. Luce,[2] James P. McNamara[3] and Nancy F. Glenn[4]

[1] *Water and Environmental Research Center, University of Alaska Fairbanks, Fairbanks, AK, USA*
[2] *U.S. Forest Service, Rocky Mountain Research Station, Boise, ID, USA*
[3] *Department of Geosciences, Boise State University, Boise, ID, USA*
[4] *Department of Geosciences, Idaho State University, Boise, ID, USA*

Abstract:

Describing the spatial variability of heterogeneous snowpacks at a watershed or mountain-front scale is important for improvements in large-scale snowmelt modelling. Snowmelt depletion curves, which relate fractional decreases in snow-covered area (SCA) against normalized decreases in snow water equivalent (SWE), are a common approach to scale-up snowmelt models. Unfortunately, the kinds of ground-based observations that are used to develop depletion curves are expensive to gather and impractical for large areas. We describe an approach incorporating remotely sensed fractional SCA (FSCA) data with coinciding daily snowmelt SWE outputs during ablation to quantify the shape of a depletion curve. We joined melt estimates from the Utah Energy Balance Snow Accumulation and Melt Model (UEB) with FSCA data calculated from a normalized difference snow index snow algorithm using NASA's moderate resolution imaging spectroradiometer (MODIS) visible (0·545–0·565 μm) and shortwave infrared (1·628–1·652 μm) reflectance data. We tested the approach at three 500 m^2 study sites, one in central Idaho and the other two on the North Slope in the Alaskan arctic. The UEB-MODIS-derived depletion curves were evaluated against depletion curves derived from ground-based snow surveys. Comparisons showed strong agreement between the independent estimates. Copyright © 2010 John Wiley & Sons, Ltd.

KEY WORDS hydrology; snow; remote sensing; arctic

Received 15 September 2009; Accepted 22 July 2010

INTRODUCTION

Redistribution of snow by wind and differential melt patterns can create complex snow distributions resulting in heterogeneous or even patchy snowpacks (Elder *et al*., 1991; Seyfried and Wilcox, 1995; Prasad *et al*., 2001; Winstral and Marks, 2002; Anderton *et al*., 2004; DeBeer and Pomeroy, 2009). Representing subgrid variability of snow-covered area (SCA) in large-scale distributed models can substantially help to adequately capture spatial snowmelt dynamics (Luce *et al*., 1998, 1999; Liston, 1999). When snowcover becomes discontinuous, parameterizations for subgrid-scale heterogeneity cause models to melt snow only for the portions of the modeled area that are covered with snow.

Snowmelt depletion curves (SDCs) are commonly used in hydrologic models to account for variability of snow within a modeled area (Anderson, 1973; Fontaine *et al*., 2002; J. Martinec *et al*., unpublished data). Conventional SDC approaches characterize the reduction in fractional SCA (FSCA) with time (Anderson, 1973; J. Martinec *et al*., unpublished data). In this approach, predicted meltwater volumes for a catchment or pixel are adjusted by the fraction of remaining SCA for any particular time step, so that the model delivers meltwater only from the portions of the modeled area that are covered with snow. To apply this approach, SCA must be monitored in real time using field measurements, photographs, or satellite imagery, or the shape of a SCA versus time curve must be known in advance. One difficulty with this approach is that the timing of melt initiation cannot be known *a proiri*.

An alternative approach relates changes in SCA to remaining snow water equivalent (SWE) in the snowpack, rather than to time explicitly (Army Corp of Engineers, 1956; Anderson, 1968, 1973; Dunne and Leopold, 1978; Ferguson, 1984; Buttle and McDonnell, 1987; Luce *et al*., 1999; J. Martinec *et al*., unpublished data). J. Martinec *et al*. (unpublished data) called this a modified depletion curve (MDC). The utility of an MDC lies in the tendency for areas with predictable sources of variability to melt in similar spatial patterns each year (Luce and Tarboton, 2004). In this modified approach, a model predicts meltwater production from an initial snowpack, and then changes in SCA are determined via the reduction in modeled SWE using a pre-determined MDC (e.g. Anderson, 1973; Stratton *et al*., 2009). The predicted aereal meltwater is then adjusted using the changes in SCA.

* Correspondence to: Joel W. Homan, Water and Environmental Research Center, University of Alaska Fairbanks, Fairbanks, AK, USA.
E-mail: jwhoman@alaska.edu

In most practical applications, the shape of an MDC for a location is not known but is assumed or used as a calibration parameter (e.g. Anderson, 1976; Sturm *et al*., 1995; Fontaine *et al*., 2002; Su *et al*., 2008). The basic theory and some testing tell us that the shape of the depletion curve is related to the spatial distribution function of snow at or near maximum accumulation (Liston, 1999; Luce *et al*., 1999; Luce and Tarboton, 2004). Unfortunately, measurements of the distribution of the snow across areas are somewhat limited, mostly to research catchments (e.g. Dunne and Leopold, 1978; Buttle and McDonnell, 1987; Donald *et al*., 1995; Sturm *et al*., 2001; Luce and Tarboton, 2004; DeBeer and Pomeroy, 2009; Molotch, 2009). While physical measurement of distributions is probably the most precise approach to estimating the distribution of snow, the expense and hazard ultimately keep them from being practical for operational snowmelt modelling at large scales.

Remote sensing in several forms has been used to estimate the spatial distribution of snow. Airborne light detection and ranging (LIDAR) represents a brute force method with some promise (e.g. Trujillo *et al*., 2007) but again with some expense and scale limitations. Reconstruction of SWE from sequential thematic mapper (TM) imagery combined with modelled melt estimates has also been used to develop spatially explicit maps of peak SWE (Cline *et al*., 1998; Molotch, 2009). In these reconstruction studies, spatially explicit SWEs at the time of maximum accumulation were estimated after the completion of ablation by modeling the amount of snow necessary to keep a pixel snow covered until a Landsat scene shows the pixel as snow free. Landsat TM data has 30-m resolution, which captures the spatial variability of complex terrain and can be used to make quantitative estimates of FSCA within each pixel (Rosenthal and Dozier, 1996; Molotch, 2009). Unfortunately, TM scenes have a return interval of 16 days, while ablation in some regions can be much shorter (Kane *et al*., 1991, 1997). This promotes the possibility that large areas, if not all the snowpack, can disappear between cloud-free TM image acquisitions, leaving substantial uncertainty about the amount of snow at a given pixel. The daily retrieval period of fractional snow coverage products from NASA's moderate resolution imaging spectroradiometer (MODIS) offers a solution for the temporal uncertainty but loses the spatially explicit information because of the 500-m resolution (Painter *et al*., 2003, 2009; Salomonson and Appel, 2004). Such coarse grained information has, however, been useful in several snowmelt modeling applications ranging from land surface model validation to data assimilation for large-scale models (Dery *et al*., 2005; Andreadis and Lettenmaier, 2006; Clark *et al*., 2006; Kolberg and Gottschalk, 2006; Su *et al*., 2008). In many cases, again, an *a priori* relationship between SWE and FSCA is required. Despite the clear potential, to date, remotely sensed data has not been used to estimate the shape of a MDC from the relationship between fractional snow coverage and the evolution of the snowpack to reduce the need to calibrate or assume depletion curve parameters.

Our goal is to evaluate the potential for using MODIS to construct modified snow depletion curves in diverse environments. We constructed MDCs using snowpack reconstruction (e.g. Cline *et al*., 1998; Molotch, 2009) concepts applied to snow-covered fractions in MODIS data and compared them to ground-based surveys in sites where the spatial variability of snow is known to occur at scales much smaller than the MODIS footprint.

METHODS

We developed MDCs for three 500 m^2 study sites closely aligned with MODIS pixels using FSCAs based on MODIS reflectance data and snowmelt modelled with the Utah Energy Balance Snow Accumulation and Melt Model (UEB) (D.G. Tarboton and C.H. Luce, unpublished data) updated with an improved surface temperature representation (You, 2004; Luce and Tarboton, 2009). The predicted hourly melt rates are applied only to the fraction that was snow covered to reconstruct the heterogeneous snowpack, allowing a matching of estimated basin average SWE to estimated basin area. Detailed field surveys throughout each study area during the ablation period were conducted to evaluate the accuracy of the modelled SWEs and FSCAs and the ultimate depletion curve.

Study areas

Three study sites were defined by the boundaries of three 500 m^2 MODIS pixels in Idaho and Alaska, USA (Figure 1). The Little Deer Point (LDP) study area (latitude 43°74′, longitude −116°12′) is located in the Dry Creek Experimental Watershed approximately 16 km northeast of the city of Boise, Idaho. LDP is located in mountainous terrain, characterized by valleys and ridges, resulting in large variations in aspect (from 80 to 300°), slope (from 2 to 78°), and elevation (from 1640 to 1850 m). LDP is within a semi-arid region of the Boise National Forest, with Douglas fir (*Pseudotsuga menziesii*), Ponderosa pine (*Pinus ponderosa*), and Aspen (*Populus tremuloides*) forests covering the valleys and hillsides and approximately 80% of LDP, while Manzanita (*Arctostaphylos columbiana*) covers most of the ridges. Climatically, the winters are cold and relatively wet, while the summers are primarily hot and dry. The majority of the annual precipitation falls as snow during the cold, wet winter months.

Imnavait Creek A and B study areas (latitude 68°30′, longitude 149°15′) are located in Imnavait Creek Watershed within the headwaters of the Kuparuk River in the foothills of the Brooks Range in northern Alaska. Imnavait Creek A ranges in elevation from roughly 880 to 900 m, has slopes between 0 and 8°, and consists of roughly 45% east-facing slopes and 55% west-facing slopes. Imnavait Creek B ranges in elevation from roughly 885 to 940 m, has slopes between 0 and 11°, and

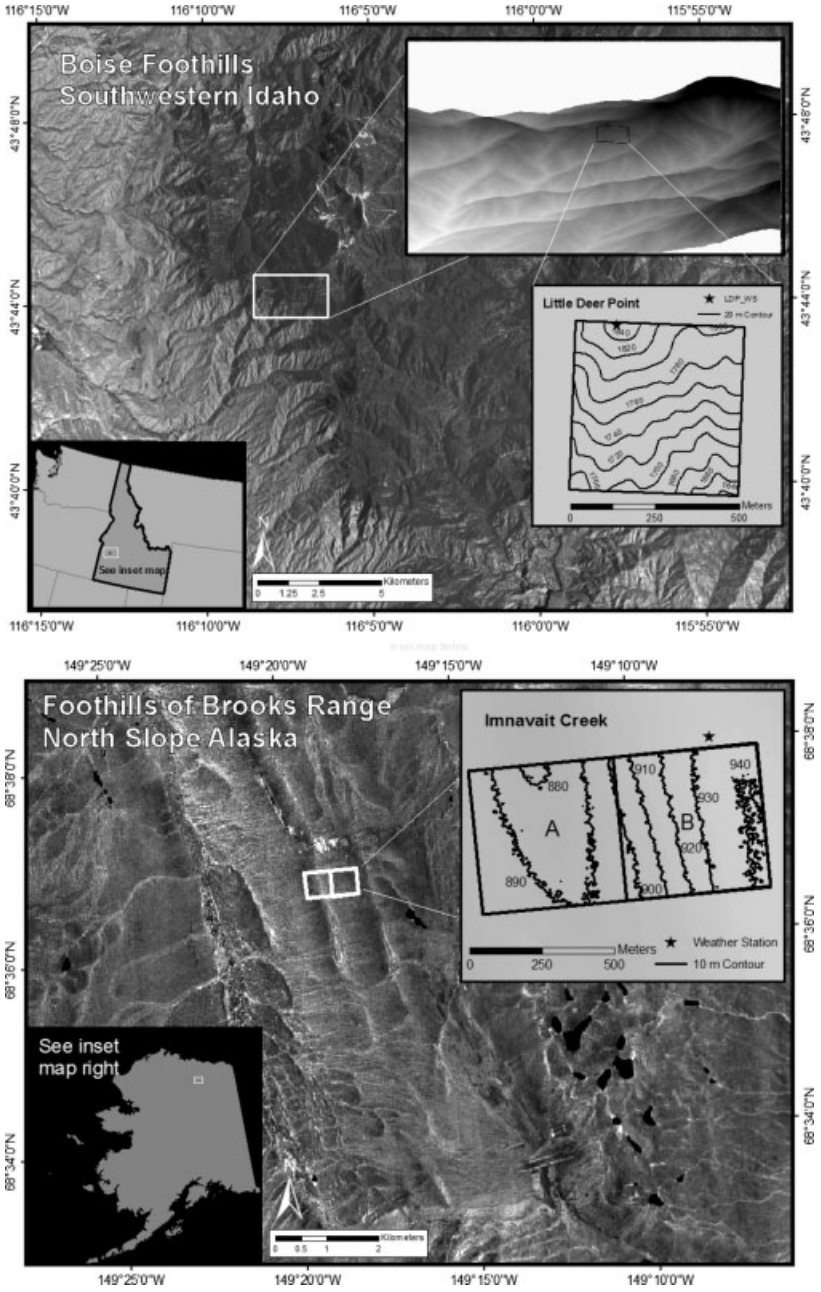

Figure 1. Location maps of the three 500 m^2 study area: Little Deer Point and Imnavait Creek A and B. digital elevation models (DEMs) and contours illustrate the local topography for the study areas. Stars represent weather stations

Table I. Spatial variability of the snowpack at maximum snow accumulation

	Little Deer Point, 2-Mar		Imnavait Creek A, 15-May		Imnavait Creek B, 12-May	
	Snow depth (cm)	Density (g/cm^3)	Snow depth (cm)	Density (g/cm^3)	Snow depth (cm)	Density (g/cm^3)
Average	67	0·19	48	0·29	44	0·26
SD	18	0·04	11	0·03	11	0·03
CV	0·28	0·22	0·24	0·11	0·25	0·12
Maximum	135	0·26	81	0·33	76	0·32
Minimum	25	0·11	23	0·23	25	0·22

consists of 20% east-facing slopes and 80% west-facing slopes. Both Imnavait Creek A and B study areas are characterized by rolling hills, completely bare of trees, continuously underlined by 250 to 300 m of permafrost, and snow covered 7–9 months of the year (Osterkamp, 1985). During the long winter, the snowcover experiences significant redistribution by wind, resulting in non-uniform snow depths, which range from 0 to 1500 mm

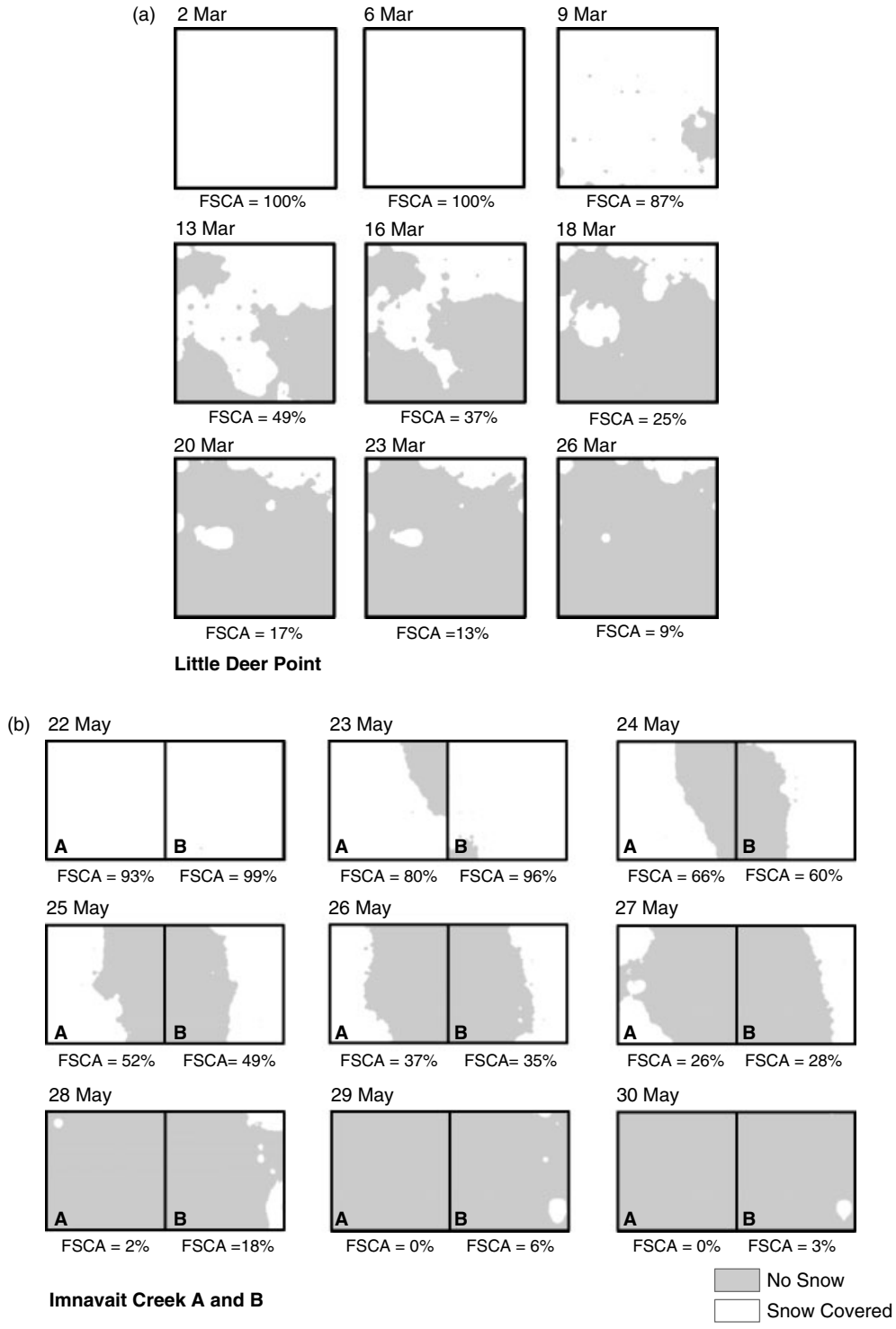

Figure 2. Ground-based FSCA mapped throughout snowmelt

Table II. Averaged ground-based data and corresponding FSCA and SWE results for Little Deer Point

Date	2-Mar	6-Mar	9-Mar	13-Mar	16-Mar	18-Mar	20-Mar	23-Mar	26-Mar
Average snow depth (cm)	67	42	27	13	8	4	3	2	1
Snow-free samples	0	0	16	62	76	91	100	105	110
FSCA (%)	1·00	1·00	0·87	0·49	0·37	0·25	0·17	0·13	0·09
Average snow ρ (g/cm^3)	0·19	0·29	0·35	0·40	0·36	0·30	0·37	0·32	0·39
Average SWE	12·73	12·12	9·38	5·09	2·69	1·21	1·06	0·71	0·46
SWE/SWE$_{max}$	1·00	0·95	0·74	0·40	0·21	0·10	0·08	0·06	0·04

Table III. Averaged ground-based data and corresponding FSCA and SWE results for Imnavait Creek A

Date	15-May	16-May	17-May	18-May	19-May	21-May	22-May	23-May	24-May	25-May	26-May	27-May	28-May
Average snow depth (cm)	48	45	41	40	40	35	29	20	14	9	5	2	0·2
Snow-free samples	0	0	0	2	2	4	8	24	41	58	76	89	118
FSCA (%)	1·00	1·00	1·00	0·98	0·98	0·97	0·93	0·80	0·66	0·52	0·37	0·26	0·02
Average snow ρ (g/cm^3)	0·29	0·25	0·28	0·29	0·27	0·29	0·30	0·32	0·34	0·27	0·30	0·38	0·34
Average SWE	13·65	11·38	11·61	11·93	10·72	10·03	8·50	6·35	4·57	2·53	1·64	0·83	0·06
SWE/SWE$_{max}$	1·00	0·83	0·85	0·87	0·79	0·73	0·62	0·47	0·33	0·19	0·12	0·06	0·00

Table IV. Averaged ground-based data and corresponding FSCA and SWE results for Imnavait Creek B

Date	12-May	15-May	16-May	17-May	18-May	19-May	21-May	22-May	23-May	24-May	25-May	26-May	27-May	28-May	29-May	30-May
Average snow depth (cm)	44	42	40	39	37	37	33	27	18	14	10	7	4	2	0·4	0·1
Snow-free samples	0	0	0	0	0	0	1	5	26	48	62	79	87	99	114	117
FSCA (%)	1·00	1·00	1·00	1·00	1·00	1·00	0·99	0·96	0·79	0·60	0·49	0·35	0·28	0·18	0·06	0·03
Average snow ρ (g/cm$_3$)	0·26	0·25	0·25	0·28	0·30	0·28	0·32	0·34	0·33	0·27	0·28	0·25	0·33	0·38	0·31	0·29
Average SWE	11·39	10·68	10·03	10·96	11·12	10·44	10·46	9·07	5·95	3·76	2·88	1·67	1·24	0·70	0·14	0·04
SWE/SWE$_{max}$	1·00	0·94	0·88	0·96	0·98	0·92	0·92	0·80	0·52	0·33	0·25	0·15	0·11	0·06	0·01	0·00

(Kane *et al*., 1991). The surface groundcover is primarily tussock sedge tundra, mosses, and low shrubs (Walker *et al*., 1989).

Estimating melt

The UEB uses a vertically lumped representation of the snowpack with two primary state variables, specifically energy content relative to a reference state of water in the ice phase at 0 °C and mass balance. The model is driven by inputs of air temperature (°C), precipitation (m/h), wind speed (m/s), relative humidity (as a fraction), daily air temperature range (max−min), and incoming and outgoing solar radiation. The required meteorological measurements were collected during ablation of 2007 at weather stations within and near the study areas (Figure 1).

Energy content calculations are based on the changes in total energy inputs and outputs, per unit time, and unit of horizontal area (i.e. in kJ m^{-2} h^{-1}):

$$\frac{\Delta U}{\Delta t} = Q_{sn} + Q_{li} + Q_p + Q_g + Q_{le} + Q_h + Q_e + Q_m \quad (1)$$

where ΔU is the change in energy content, Δt the change in time; Q_{ns} the net shortwave radiation, Q_{li} the incoming longwave radiation, Q_p the advected heat from precipitation, Q_g the ground heat flux, Q_{le} the outgoing longwave radiation, Q_h the sensible heat flux, Q_e the latent heat flux due to sublimation/condensation, and Q_m the advected heat removed by meltwater. The mass balance calculations are based on the changes in water content per unit time (all in m/h of water equivalence):

$$\frac{\Delta W}{\Delta t} = P_r + P_s - M - E \quad (2)$$

where ΔW is the change in water CONTENT, P_r the rainfall rate, P_s the snowfall rate, M the meltwater outflow from the snowpack, and E the sublimation from the snowpack (D.G. Tarboton and C.H. Luce, unpublished data).

Remotely sensed FSCA

MODIS is an imaging spectroradiometer onboard the Earth Observing System Terra and Aqua satellites, which were launched in 1999 and 2002, respectively. MODIS provides 12-bit radiometric sensitivity in 36 discrete, narrow spectral bands ranging in wavelength from the visible to thermal infrared (0·4–14·4 μm). Two of the bands are imaged at a nominal resolution of 250 m at nadir, 5 bands at 500 m and the remaining 29 at 1 km. Global coverage every 1–2 days is obtained using a ±55° cross-track scanning mirror located 705 km above Earth's surface, which obtains a 2030 by 2330 km swath (National Snow and Ice Data Center, 2006).

To map snowcover and subsequently determine rates of snowcover depletion using satellite remote sensing data, snow must be distinguished from other surface cover and from clouds. Reflectance of non-snow surface features such as rock outcrops, scattered trees, and other

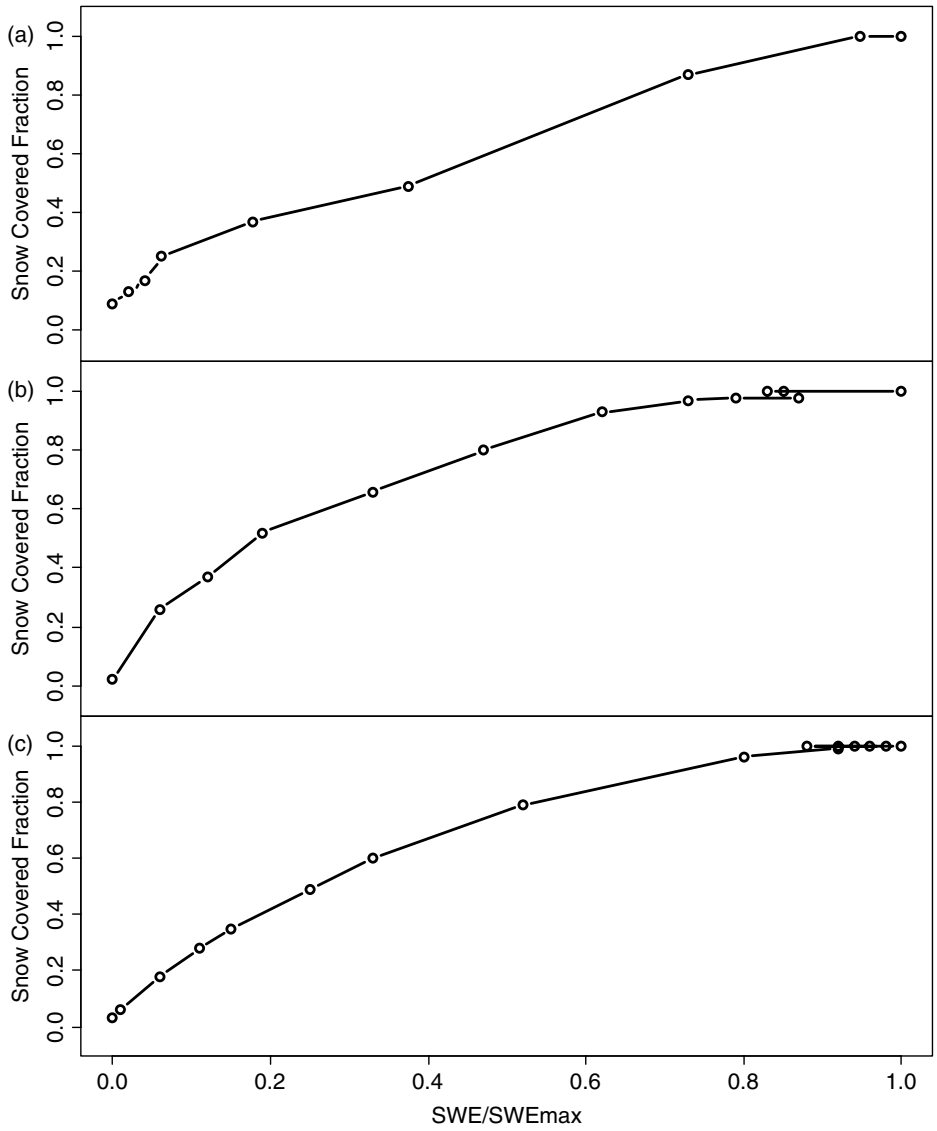

Figure 3. Ground-based depletion curves for a) Little Deer Point, b) Imnavait Creek A, and c) Imnavait Creek B

vegetation are considerably less than the reflectance of snow. Snow/cloud discrimination is, however, more problematic because in visible (∼0·4–0·7 μm), near-infrared (∼0·7–1·4 μm), and thermal infrared (∼3·0–15 μm) wavelengths, snow and clouds have similar reflected and emitted radiance (Dozier *et al*., 1981; Dozier, 1984, 1989; Hall *et al*., 1992). In the shortwave infrared (SWIR; ∼1·5–1·7 μm), clouds exhibit a relatively high reflectivity, whereas snow areas have an extremely low reflectivity (Rango and Itten, 1976). For snowcover monitoring, such a contrast can be utilized to significantly reduce most of the ambiguities between snow and clouds (Rango and Itten, 1976; Dozier, 1989; Hall *et al*., 1995).

The normalized difference snow index (NDSI) developed by Dozier (1989), but termed by Riggs *et al*. (1994), makes use of the differences between visible and SWIR wavelengths to identify snowcover and discriminate snow from clouds. For MODIS data, the NDSI is expressed as

$$\mathrm{NDSI} = \frac{\text{band 4} - \text{band 6}}{\text{band 4} + \text{band 6}} \tag{3}$$

where MODIS band 4 (0·545–0·565 μm) is visible green and MODIS band 6 (1·628–1·652 μm) is SWIR (Riggs *et al*., 1994; Hall *et al*., 1995, 2002; Justice *et al*., 2002).

Salomonson and Appel (2004) developed a fractional snowcover algorithm by populating 500-m-resolution MODIS scenes with 30-m Landsat scenes for three snow-covered sites during the winter of 2000/2001. MODIS-based NDSI values were regressed against the fraction of the pixel covered by snowy Landsat scenes:

$$\mathrm{FSCA} = A + B \times \mathrm{NDSI} \tag{4}$$

where $A = 0{\cdot}06$ and $B = 1{\cdot}21$ (Salomonson and Appel, 2004). The depletion of a SCA inferred from MODIS using Equation (4) was validated by Dery *et al*. (2005) in the Kuparuk River basin in northern Alaska, approximately 3 km from our Imnavait Creek A and B study areas.

MODIS Level 1B Calibrated Reflectance −500-m (MOD02HKM) data were acquired everyday for the duration of the 2007 snowmelt for all three study areas.

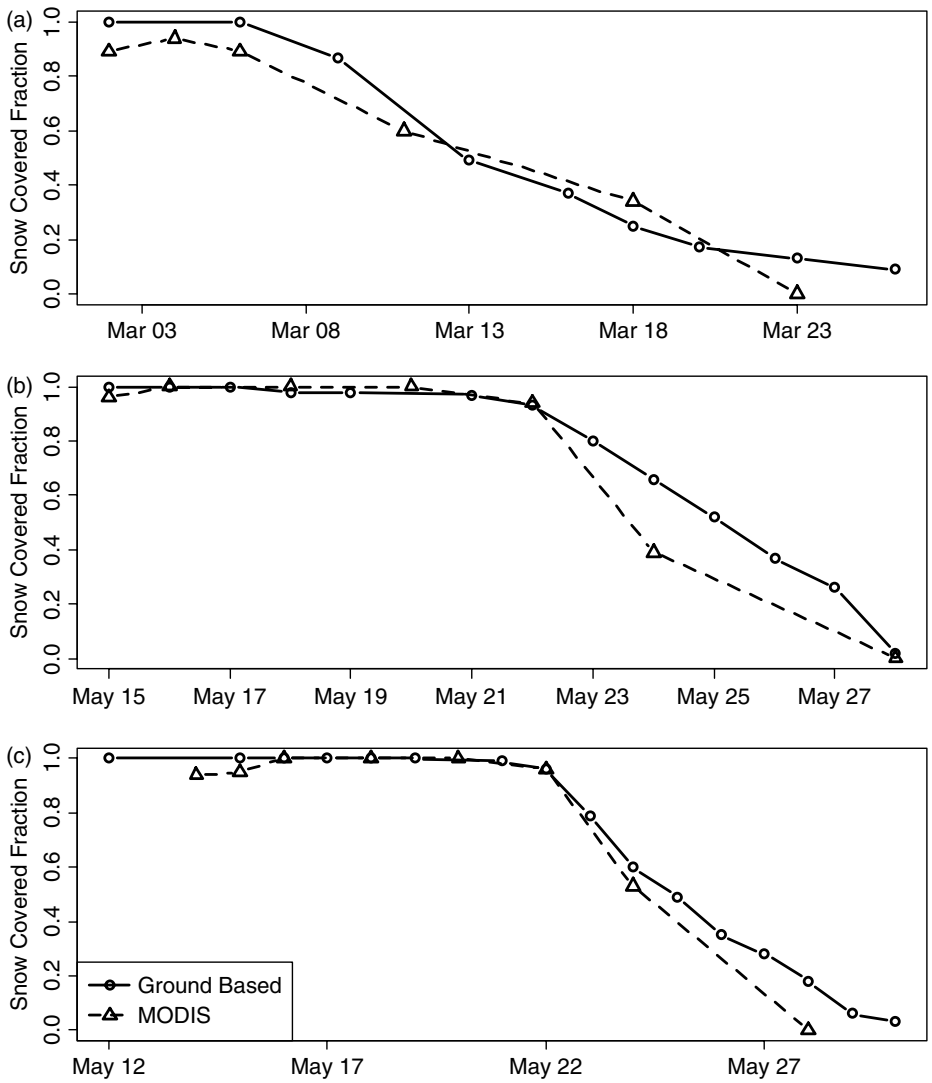

Figure 4. Ground-based FSCA ($FSCA_{ground}$) evaluated against MODIS-based NDSI-derived FSCA ($FSCA_{NDSI}$) for a) Little Deer Point, b) Imnavait Creek A, and c) Imnavait Creek B

The images were georeferenced and the alignment of the 500-m MODIS pixels and 500-m study areas was verified by overlaying georeferenced MODIS images with vector files of the study areas. Images with cloud cover over the study areas were not used. In LDP, 6 of 26 days of snowmelt were cloud free. In Imnavait Creek A, 7 of the 14 days of snowmelt were cloud free and 8 of the 15 days of snowmelt were cloud free in Imnavait Creek B. Once the alignment of the pixels were evaluated, MODIS-based NDSI-derived FSCA ($FSCA_{NDSI}$) values were calculated using Equations (3) and (4).

At LDP, these equations produced some severe errors in the SCA estimate. For example, the Salomonson–Appel equations never detected full snowcover at LDP and significantly underestimated the snow fraction when snowcovers were continuous (FSCA > 50%), with differences as great as 33% from observations. A possible explanation is interference from the tree canopy. In both Imnavait Creek A and B study areas, FSCA values were much better estimated using the general equations. We corrected the LDP FSCA estimates following the procedures of Dery *et al.* (2005) for this exercise to examine, in principle, the utility of remotely sensed data for estimating depletion curves. Recently developed spectral mixing methods to estimate FSCA are proposed to correct the problems we encountered using the older methods (Dozier *et al.*, 2008; Painter *et al.*, 2009). Note that information for improving the calibration of MODIS data could still be obtained remotely (e.g. periodic TM data) or at much lower field effort than the complete depth surveys usually used in research practice.

Constructing the depletion curve

The point snowmelt model provided the depth of potential melt of a snow-covered point for each day (ΔSWE). The total potential melt between successive MODIS images was multiplied by the average $FSCA_{NDSI}$ ($\overline{FSCA_{ndsi}}$) between those corresponding images to produce area-average loss estimate for that interval:

$$\text{Melt} = \Delta\text{SWE} \times \overline{\text{FSCA}_{\text{NDSI}}} \quad (5)$$

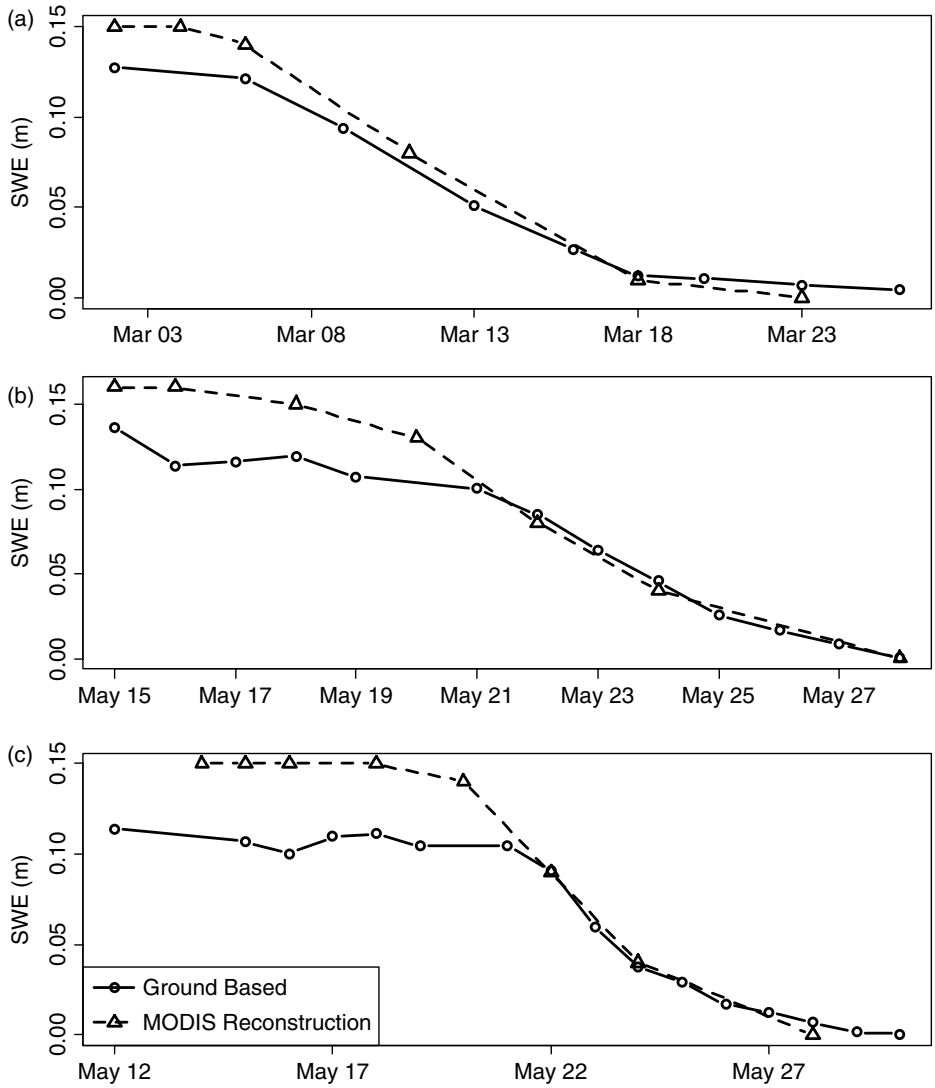

Figure 5. UEB/MODIS reconstructed SWE compared to ground snow surveys at a) Little Deer Point, b) Imnavait Creek A, and c) Imnavait Creek B

SWE–time depletion curves for each study area were constructed by successively adding the corrected melt depths from Equation (5) back in time. This sums losses on any SCAs within a pixel in a method similar to those by Cline *et al*. (1998) and Molotch (2009) but applied to fractions of a pixel rather than an entire pixel. The primary output of interest from the UEB modeling is the ΔSWE value, not the specific estimates of SWE for a given snow-covered point within the study area, which could be arbitrarily deep.

Ground-based depletion curve

Snowpack field studies focused primarily on the maximum SWE accumulation of the 2006–2007 winter and the snowmelt that followed. Field activities started at the beginning of March for LDP and at the beginning of May for the Imnavait Creek study areas because, by then, the snowpack contained nearly all precipitation that was going to fall during the winter months (less sublimation). In LDP, the surveys were completed roughly every 3 days between March 2 and 26. Surveys within the Imnavait Creek A and B were conducted from May 4 to 30, starting with measurements every other day during final snow accumulation and concluding with daily measurements during snowmelt.

The end-of-winter snow surveys were conducted throughout the study areas to determine snow depth as well as vertically integrated density, SWE, and FSCA. Snow depths, totalling 121 per study area, were measured every 50 m along a grid throughout the 500 m^2 study areas by probing the snow with a staff incremented in centimeters. The snowpack densities were obtained using snow cores taken at different slopes and aspects. In LDP, a federal sampler with hanging scale was used, and in the Imnavait Creek A and B, an Adirondack fibreglass snow sampler with a digital scale was used. Different snow-coring devices were used due to the differences between mountain and arctic snowpack properties. Fifteen snow cores were collected per survey within each study area during high snow coverage, but as the snowcover decreased, fewer cores were collected. Fewer density measurements were collected compared to snow depths because in heterogeneous snowpacks, snow depth is more variable than density (Benson and Sturm, 1993).

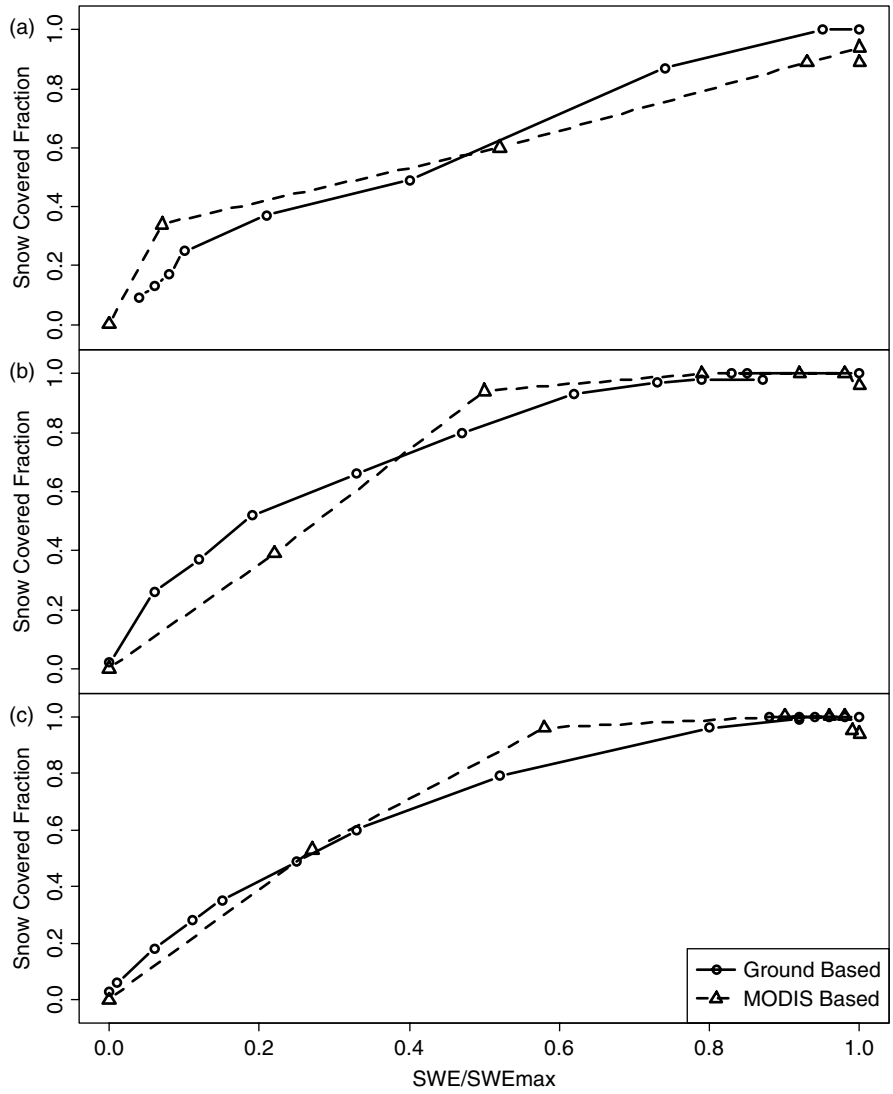

Figure 6. Depletion curves derived from remotely sensed data compared to ground observations for a) Little Deer Point, b) Imnavait Creek A, and c) Imnavait Creek B

The SWE was estimated as

$$\mathrm{SWE} = (\mathrm{SD} \times \rho_S)/\rho_W \quad (6)$$

where ρ_s is the average snow density from the 15 snow core samples, ρ_w the water density, and SD the average of 121 snow depths. The FSCA was defined as

$$\mathrm{FSCA} = \mathrm{Count}\ (\mathrm{SD} > 0{\cdot}0\ \mathrm{cm})/n \quad (7)$$

where n is the number of snow depth measurements.

RESULTS AND DISCUSSION

Ground-based observations and depletion curves

At the time of maximum snow accumulation, the average, maximum, and minimum snowdepth at LDP were 67, 135, and 25 cm, respectively (Table I). Snowcover decreased from 100 to 87% between March 6 and 9 and further decreased to 9% by March 26 (Figure 2). Average snow density increased from 0·19 and 0·40 g/cm^3 between March 2 and 13 and then fluctuated between 0·4 and 0·3 g/cm^3 for the remainder of ablation (Tables II–IV). No snow accumulation interrupted the depletion until snowcover was reduced to 9%, when a storm deposited 2 in. of new snow over the entire study area. For simplicity, we have eliminated this event from the analysis. The ground-based MDC for LDP is a fairly linear relationship (Figure 3), suggesting a relatively heterogenous accumulation and melt.

At Imnavait Creek A, the average, maximum, and minimum snow depths at the time of maximum snow accumulation were 48, 81, and 23 cm, respectively (Table I). Snowcover decreased from 100 to 0% between May 22 and 29 (Figure 2). The east side of the study area (west-facing slope and valley bottom) melted first, followed by the west side (east-facing slope). The average snow density fluctuated between 0·29 and 0·38 g/cm^3 during ablation (Table II–IV). No new snow interrupted ablation. The ground-based MDC was horizontal in the early melt period indicating loss of SWE with little to no loss of SCA (Figure 3). At approximately 85% SWE, the curve

became concave down, indicating progressively faster loss in SCA as SWE reduced. This shape is consistent with low heterogeneity.

At Imnavait Creek B at the time of maximum snow accumulation, the average, maximum, and minimum snow depths were 44, 76, and 25 cm, respectively (Table I). Snowcover decreased from 100% on May 22 to 3% on May 30 (Figure 2). The west side of the study area (west-facing slope) melted first, followed by the ridge top in the centre and subsequently the east side (east-facing slope). A drift persisted on the east-facing slope after our sampling ended. The average snow density fluctuated between 0·25 and 0·35 g/cm^3 during ablation (Table II–IV). No new snow interrupted ablation. The ground-based MDC was concave downward throughout the melt period (Figure 3).

Remotely sensed depletion curve

Comparison between ground-based FSCA ($FSCA_{ground}$) and MODIS-based NDSI-derived FSCA ($FSCA_{NDSI}$) shows reasonable agreement (Figure 4). While LDP required some correction to yield this fit, as discussed earlier, no correction was done for either Imnavait Creek site. An important point, however, is that our results must be tempered by the assumption that reasonably accurate estimates of FSCA can be obtained from remote sensing. Fortunately, recent work in this area shows promise (Dozier *et al*., 2008; Painter *et al*., 2009) and is likely a better candidate for future efforts than the linear NDSI model.

The reconstructed SWE over time for each study area overestimated the ground measured SWEs during the early portion of the melt period (Figure 5). The errors were roughly proportional to the estimate, meaning that a 10% error in estimate average SWE would yield less error when the shape was normalized to the maximum estimated SWE. The $FSCA_{NDSI}$ (Figure 4) and distributed UEB-modeled SWE (Figure 5) estimates were normalized and plotted against each other to develop remotely sensed MDCs. For all three study sites, the remotely sensed MDC had a similar shape to the ground-based curve (Figure 6), confirming the potential to use remote sensing information combined with meteorological data to provide an independent estimate of snow depletion relationships from those that might be assumed or calibrated.

CONCLUSION

This study investigated a method for improving snowmelt estimates for greater areas of the landscape through the development of a remotely sensed depletion curve without requiring field-based surveys. We demonstrated that MDCs developed with MODIS-based NDSI-derived FSCA and melt estimates from a snowmelt model were comparable to the results from ground-based observations of the MDC for three 500-m square study areas. The remotely sensed MDC offers an exciting advancement as a method for researchers to more accurately estimate the spatial and temporal variability of snowmelt across much larger areas. There is also a clear potential use in independent calibration for operational hydrologic models (e.g. Anderson, 1973) or data assimilation procedures (e.g. Andreadis and Lettenmaier, 2006; Clark *et al*., 2006; Kolberg and Gottschalk, 2006; Su *et al*., 2008). Important future uses of the approach would be to explore environmental factors controlling depletion curve shape and temporal stability of depletion curves from year-to-year.

ACKNOWLEDGEMENTS

We are grateful to M. Thoma, P. Aishlin, B. Hoffman, C. van Breukelen, and E. Trochim for field assistance and to the Toolik Field Station for logistical support. This work was supported by NSF-Idaho EPSCoR Program and the National Science Foundation under award number EPS-0447689 and EPS-0814387, and by the Idaho Space Grant Consortium.

REFERENCES

Anderson EA. 1968. Development and testing of snow pack energy balance equations. *Water Resources Research* **4**: 19–37.

Anderson EA. 1973. *National Weather Service River Forecast System—Snow Accumulation and Ablation Model*. United States Department of Commerce Publication: Springfield, PA, USA.

Anderson EA. 1976. *A Point Energy and Mass Balance Model of a Snow Cover* Silver Spring, Md.: U.S. Department of Commerce, National Oceanic and Atmospheric Administration, National Weather Service, Office of Hydrology.

Anderton SP, White SM, Alvera B. 2004. Evaluation of spatial variability in snow water equivalent for a high mountain catchment. *Hydrological Processes* **18**(3): 435–453. DOI: 10.1002/hyp.1319.

Andreadis KM, Lettenmaier DP. 2006. Assimilating remotely sensed snow observations into a macroscale hydrology model. *Advances in Water Resources* **29**(6): 872–886.

Benson CS, Sturm M. 1993. Structure and wind transport of seasonal snow on the Arctic Slope of Alaska. *Annals of Glaciology* **18**: 261–267.

Buttle JM, McDonnell JJ. 1987. Modelling the areal depletion of snowcover in a forested catchment. *Journal of Hydrology* **90**: 43–60.

Clark MP, Slater AG, Barrett AP, Hay LE, McCabe GJ, Rajagopalan B, Leavesley GH. 2006. Assimilation of snow covered area information into hydrologic and land-surface models. *Advances in Water Resources* **29**(8): 1209–1221.

Cline DW, Bales RC, Dozier J. 1998. Estimating the spatial distribution of snow in mountain basins using remote sensing and energy balance modeling. *Water Resources Research* **34**(5): 1275–1285.

DeBeer CM, Pomeroy JW. 2009. Modelling snow melt and snowcover depletion in a small alpine cirque, Canadian Rocky Mountains. *Hydrological Processes* **23**(18): 2584–2599.

Dery SJ, Salomonson VV, Stieglitz M, Hall DK, Appel I. 2005. An approach to using snow areal depletion curves inferred from MODIS and its application to land surface modelling in Alaska. *Hydrological Processes* **19**(14): 2755–2774. DOI: 10.1002/hyp.5784.

Donald JR, Soulis ED, Kouwen N, Pietroniro A. 1995. A land cover-based snow cover representation for distributed hydrologic models. *Water Resources Research* **31**(4): 995–1009.

Dozier J. 1984. Snow reflectance from Landsat-4 thematic mapper. *IEEE Transactions on Geoscience and Remote Sensing* **22**(3): 323–328.

Dozier J. 1989. Estimation of properties of alpine snow from landsat thematic mapper. *Advances in Space Research* **9**(1): 207–215.

Dozier J, Painter TH, Rittger K, Frew JE. 2008. Time-space continuity of daily maps of fractional snow cover and albedo from MODIS. *Advances in Water Resources* **31**(11): 1515–1526. DOI: 10.1016/j.advwatres.2008.08.011.

Dozier J, Schneider SR, McGinnis DF Jr. 1981. Effect of grain size and snowpack water equivalence on visible and near-infrared satellite

observations of snow. *Water Resources Research* **17**(4): 1213–1221. DOI: 10.1029/WR017i004p01213.

Dunne T, Leopold LB. 1978. *Water in Environmental Planning*. W.H. Freeman: New York.

Elder K, Dozier J, Michaelsen J. 1991. Snow accumulation and distribution in an alpine watershed. *Water Resources Research* **27**(7): 1541–1552.

Engineers, A. C. o. 1956. U.S. Army Corps of Engineers. 1956. Snow Hydrology, North Pacific Division, Porland, OR.

Ferguson RI. 1984. Magnitude and modeling of snowmelt runoff in the Cairngorm Mountains, Scotland. *Hydrological Sciences Journal—Journal Des Sciences Hydrologiques* **29**(1): 49–62.

Fontaine TA, Cruickshank TS, Arnold JG, Hotchkiss RH. 2002. Development of a snowfall-snowmelt routine for mountainous terrain for the soil water assessment tool (SWAT). *Journal of Hydrology* **262**(1–4): 209–223.

Hall DK, Foster JL, Chang ATC. 1992. Reflectance of snow measured in situ and from space in sub-Arctic areas in Canada and Alaska. *IEEE Transactions on Geoscience and Remote Sensing* **30**(3): 634–637.

Hall DK, Riggs GA, Salomonson VV. 1995. Development of methods for mapping global snow cover using moderate resolution imaging spectroradiometer data. *Remote Sensing of Environment* **54**(2): 127–140. DOI: 10.1016/0034-4257(95)00137-P.

Hall DK, Riggs GA, Salomonson VV, DiGirolamo NE, Bayr KJ. 2002. MODIS snow-cover products. *Remote Sensing of Environment* **83**(1–2): 181–194.

Justice CO, Townshend JRG, Vermote EF, Masuoka E, Wolfe RE, Saleous N, Roy DP, Morisette JT. 2002. An overview of MODIS land data processing and product status. *Remote Sensing of Environment* **83**(1–2): 3–15.

Kane DL, Gieck RE, Hinzman LD. 1997. Snowmelt modeling at amall Alaskan arctic watershed. *Journal of Hydrologic Engineering* **2**(4): 204–210.

Kane DL, Hinzman LD, Benson CS, Liston GE. 1991. Snow hydrology of a headwater arctic basin. 1. Physical measurements and process studies. *Water Resources Research* **27**(6): 1099–1109.

Kolberg SA, Gottschalk L. 2006. Updating of snow depletion curve with remote sensing data. *Hydrological Processes* **20**(11): 2363–2380. DOI: 10.1002/hyp.6060.

Liston GE. 1999. Interrelationship among snow distribution, snowmelt, and snow cover depletion: implication for atmospheric, hydrologic, and ecologic modeling. *Journal of Applied Meteorology* **38**: 1474–1487.

Luce CH, Tarboton DG. 2004. The application of depletion curves for parameterization of subgrid variability of snow. *Hydrological Processes* **18**(8): 1409–1422.

Luce CH, Tarboton DG. 2009. Evaluation of alternative formulae for calculation of surface temperature in snowmelt models using frequency analysis of temperature observations. *Hydrology and Earth System Science Discussions* **6**(3): 3863–3890.

Luce CH, Tarboton DG, Cooley KR. 1998. The influence of the spatial distribution of snow on basin-averaged snowmelt. *Hydrological Processes* **12**(10–11): 1671–1683.

Luce CH, Tarboton DG, Cooley KR. 1999. Subgrid parameterization of snow distribution for an energy and mass balance snow-cover model. *Hydrological Processes* **13**: 1921–1933.

Molotch NP. 2009. Reconstructing snow water equivalent in the Rio Grande headwaters using remotely sensed snow cover data and a spatially distributed snowmelt model. *Hydrological Processes* **23**(7): 1076–1089. DOI: 10.1002/hyp.7206.

NSIDC. 2006. National Snow and Ice Data Center. http://nsidc.org/data/modis/order.html.

Osterkamp TE. 1985. *Temperature Measurements in Permafrost*. Fairbanks, Alaska. State of Alaska, department of transportation and public facilities, division of planning and programming, research section.

Painter TH, Dozier J, Roberts DA, Davis RE, Green RO. 2003. Retrieval of subpixel snow-covered area and grain size from imaging spectrometer data. *Remote Sensing of Environment* **85**(1): 64–77. DOI: 10.1016/s0034-4257 (02) 00187-6.

Painter TH, Rittger K, McKenzie C, Slaughter P, Davis RE, Dozier J. 2009. Retrieval of subpixel snow covered area, grain size, and albedo from MODIS. *Remote Sensing of Environment* **113**(4): 868–879. DOI: 10.1016/j.rse.2009.01.001.

Prasad R, Tarboton DG, Liston GE, Luce CH, Seyfried MS. 2001. Testing a blowing snow model against distributed snow measurements at Upper Sheep Creek, Idaho, United States of America. *Water Resources Research* **37**(5): 1341–1356.

Rango A, Itten KI. 1976. Satellite potentials in snowcover monitoring and runoff prediction. *Nordic Hydrology* **7**: 206–230.

Riggs GA, Hall DK, Salomonson VV. 1994. A snow index for the Landsat thematic mapper and moderate resolution imaging spectroradiometer. *Paper presented at the Geoscience and Remote Sensing Symposium, 1994. IGARSS'94. Surface and Atmospheric Remote Sensing: Technologies, Data Analysis and Interpretation, International*.

Rosenthal W, Dozier J. 1996. Automated mapping of montane snow cover at subpixel resolution from the Landsat thematic mapper. *Water Resources Research* **32**(1): 115–130.

Salomonson VV, Appel I. 2004. Estimating fractional snow cover from MODIS using the normalized difference snow index. *Remote Sensing of Environment* **89**(3): 351–360. DOI: 10.1016/j.rse.2003.10.016.

Seyfried MS, Wilcox BP. 1995. Scale and the nature of spatial variability—field examples having implications for hydrologic modeling. *Water Resources Research* **31**(1): 173–184.

Stratton BT, Sridhar V, Gribb MM, McNamara JP, Narasimhan B. 2009. Modeling the spatially varying water balance processes in a semiarid mountainous watershed of Idaho. *JAWRA Journal of the American Water Resources Association* **45**(6): 1390–1408.

Sturm M, Holmgren J, Liston GE. 1995. A seasonal snow cover classification system for local to global applications. *Journal of Climate* **8**(5): 1261–1283.

Sturm M, McFadden JP, Liston GE, Chapin Iii FS, Racine CH, Holmgren J. 2001. Snow–shrub interactions in Arctic Tundra: a hypothesis with climatic implications. *Journal of Climate* **14**(3): 336–344. DOI:10.1175/1520-0442(2001)014<0336:SSIIAT>2.0.CO;2.

Su H, Yang Z-L, Niu G-Y, Dickinson RE. 2008. Enhancing the estimation of continental-scale snow water equivalent by assimilating MODIS snow cover with the ensemble Kalman filter. *Journal of Geophysical Research* **113**(D8): D08120.

Trujillo E, Ramírez JA, Elder KJ. 2007. Topographic, meteorologic, and canopy controls on the scaling characteristics of the spatial distribution of snow depth fields. *Water Resources Research* **43**(7): W07409.

Walker DA, Binnian E, Evans BM, Lederer ND, Nordstrand E, Webber PJ. 1989. Terrain, vegetation and landscape evolution of the R4D research site, Brooks-Range-Foothills, Alaska. *Holarctic Ecology* **12**(3): 238–261.

Winstral A, Marks D. 2002. Simulating wind fields and snow redistribution using terrain-based parameters to model snow accumulation and melt over a semi-arid mountain catchment. *Hydrological Processes* **16**(18): 3585–3603.

You J. 2004. *Snow hydrology: the parameterization of subgrid processes within a physically based snow energy and mass balance model*. PhD dissertation, Utah State University, Logan, Utah, 188pp.

